NANO · MICRO small
www.small-journal.com

Facile Preparation of Full-Color Tunable Room Temperature Phosphorescence Cellulose via Click Chemistry

Qian Gao, Meichao Shi, Mingxing Chen, Xiang Hao, Gegu Chen, Jing Bian, Baozhong Lü, Junli Ren, and Feng Peng**

Sustainable long-lived room temperature phosphorescence (RTP) materials with color-tunable afterglows are attractive but rarely reported. Here, cellulose is reconstructed by directed redox to afford ample active hydroxyl groups and water-solubility; arylboronic acids with various π conjugations can be facilely anchored to reconstructed cellulose via click chemistry within 1 min in pure water, resulting in full-color tunable RTP cellulose. The rigid environment provided by the B—O covalent bonds and hydrogen bonds can stabilize the triplet excitons, thus the target cellulose displays outstanding RTP performances with the lifetime of 2.67 s, phosphorescence quantum yield of 9.37%, and absolute afterglow luminance of 348 mcd m^{-2}. Furthermore, due to the formation of various emissive species, the smart RTP cellulose shows excitation- and time-dependent afterglows. Taking advantages of sustainability, ultralong lifetime, and full-color tunable afterglows, et al, the environmentally friendly RTP cellulose is successfully used for nontoxic afterglow inks, delay lighting, and afterglow display.

1. Introduction

Organic room temperature phosphorescence (RTP) materials with ultralong and color-tunable afterglows have attracted widespread attention due to their potential applications in light emitting diodes,[1] visual decoration,[2] anticounterfeiting,[3] sensing,[4] and bioimaging.[5] Long-lived afterglow of organic molecules is known as phosphorescence from radiative decay of triplet excitons. To achieve satisfying RTP, boosting singlet-triplet intersystem crossing (ISC) and reducing non-radiative transitions are essential. To this end, heteroatom and/or heavy atoms effect,[6] crystallization,[7] supramolecular assembly,[8] polymer encapsulation,[4b,9] and some other helpful approaches were developed to promote triplet excitons population and suppress the molecular motion dissipations.[10] The past few years have witnessed the significant progress of organic RTP materials based on these principles.[11] However, major organic RTP materials are prepared by complicated and time-consuming chemical synthesis, accompanied by the consumption of toxic organic solvents and non-degradable petroleum polymer.[12] Moreover, RTP materials with color-variable afterglows in response to both excitation wavelength (λ_{ex}) and delayed time are rarely reported. Thus, the development of new organic RTP materials to address the above issues is of significant importance to practically apply phosphorescent materials and reduce the environmental pollution.

Cellulose is the most abundant sustainable and biodegradable polymer in nature, which has been found to emit weak phosphorescence itself via a clusterization-triggered emission (CTE) phenomenon recently.[13] Sustainable RTP material that does not harm the environment can be prepared by cellulose. Impressively, Zhang et al have successfully obtained a series of RTP cellulose by introducing imidazolium cation or anionic substituents into the cellulose chain.[14] However, the reported RTP cellulose displayed unsatisfactory phosphorescence performance and monotonous afterglow color when compared with petroleum polymer based RTP materials.[3c,4b,15] Theoretically, cellulose with sufficient hydroxyl groups in glucose C2, C3, and C6 positions can replace petroleum polymer (such as the most used poly(vinyl alcohol) (PVA)) to constructed RTP materials by physical or chemical encapsulation. However, cellulose is infusible and insoluble, and the ortho hydroxyl groups (C2 and C3 positions) of cellulose are of low reactivity, which are the primary obstacles to construct RTP cellulose. Very recently, we adopted a directed redox strategy to transform the C2 and C3 secondary hydroxyl groups of cellulose into primary hydroxyl groups with high

Q. Gao, M. Shi, X. Hao, G. Chen, J. Bian, B. Lü, F. Peng
Beijing Key Laboratory of Lignocellulosic Chemistry
MOE Engineering Research Center of Forestry Biomass Materials and Energy
College of Materials Science and Technology
Beijing Forestry University
Beijing 100083, China
E-mail: lvbaozhong@bjfu.edu.cn; fengpeng@bjfu.edu.cn

M. Chen
Analytical Instrumentation Center of Peking University
Peking University
Beijing 100871, China

B. Lü, J. Ren
State Key Laboratory of Pulp and Paper Engineering
South China University of Technology
Guangzhou 510640, China

F. Peng
State Key Laboratory of Efficient Production of Forest Resources
Beijing 100083, China

The ORCID identification number(s) for the author(s) of this article can be found under https://doi.org/10.1002/smll.202309131

DOI: 10.1002/smll.202309131

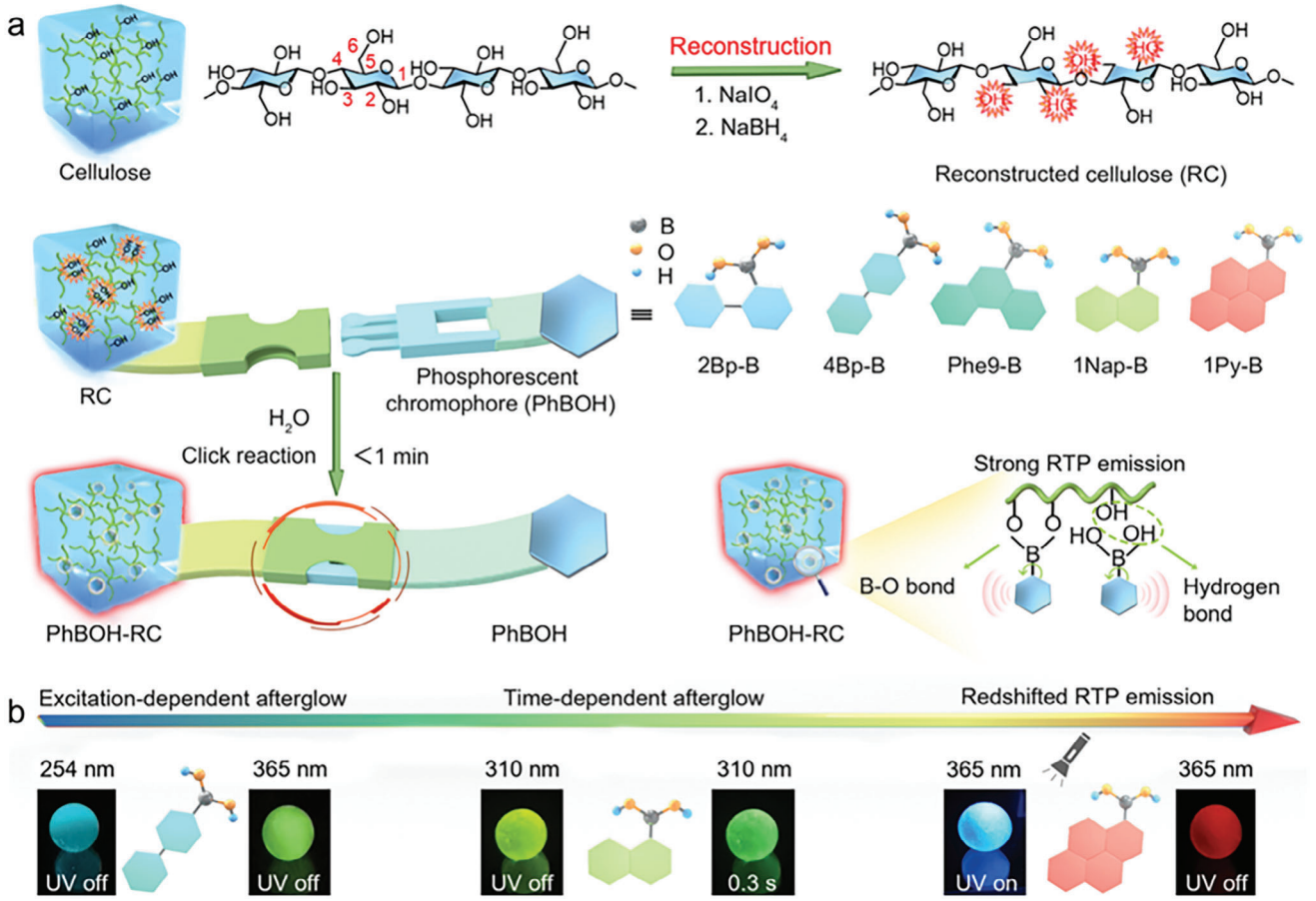

Figure 1. Construction of full-color tunable RTP cellulose. a) Schematic diagram of the preparation of full-color tunable RTP cellulose via click reaction and corresponding RTP mechanism. b) Full-color tunable and excitation/time-dependent afterglows of smart RTP cellulose.

reactivity.[16] We reason that the reconstructed cellulose (RC) is an ideal substrate for constructing long-lived and color-tunable RTP materials on account of 1) RC with abundant hydroxyls can provide a rigid microenvironment to suppress the nonradiative transitions of the triplet excitons, 2) RC is water soluble and its active primary hydroxyl groups can covalently react with chromophores to impede molecular motions, and 3) RC can offer multifarious interactions to form various emissive species for color-tunable RTP.

B—O covalent reaction has been proven to be a rapid and efficient strategy for constructing RTP materials using polymer polyols. For example, Lu et al have developed polyvinyl alcohol (PVA)-based RTP materials by the B—O click reaction;[17] Li et al subsequently developed PVA-based stimulus responsive RTP materials by similarly taking advantage of the B—O covalent reaction;[15,18] Yuan et al recently developed sodium alginate-based RTP materials with multi-responsive afterglows.[19] However, it should be noting that the above polymer substrates are water soluble. When it comes to cellulose, the B—O covalent reaction is theoretically inapplicable due to the poor accessibility. Most previous works require complex and time-consuming chemical synthesis accompanied by the consumption of toxic organic solvents to prepare RTP cellulose.[14,20] It remains scientific challenges to develop RTP celluloses using a facile and eco-friendly protocol, especially those with color-tunable afterglows.

Here, we developed a series of smart afterglow RTP cellulose through facile B—O click reaction between arylboronic acids with various π conjugations and RC matrix within 1 min under ambient conditions (**Figure 1**a). The B—O covalent bonds and hydrogen bonds of arylboronic acids-RC (the samples are denoted as 2Bp-B-R, 4Bp-B-R, Phe9-B-R, 1Nap-B-R, and 1Py-B-R, respectively) can restrain the motions of chromophores and enhance ISC, thus facilitating the RTP emission. These five arylboronic acids were chosen for the reason that by modulating the conjugated degree of arylboronic acids, the afterglow colors can be finely regulated from blue to green, then to red (Figure 1b). Among which, Phe9-B-R shows the striking lifetime of 2.67 s, phosphorescence quantum yield of 9.37%, and absolute afterglow luminance of 348 mcd m^{-2}. Remarkably, all arylboronic acids-RC samples display prominent excitation-dependent afterglows due to the formation of various emissive species. More attractively, Phe9-B-R and 1Nap-B-R simultaneously exhibit significant time-dependent afterglows (Figure 1b). In comparison, the same reaction of arylboronic acids and pristine cellulose will lead to inferior RTP performance of the corresponding products due to the insufficient covalent stabilizing. In view of the excellent sustainability, water-solubility, ultralong as well as

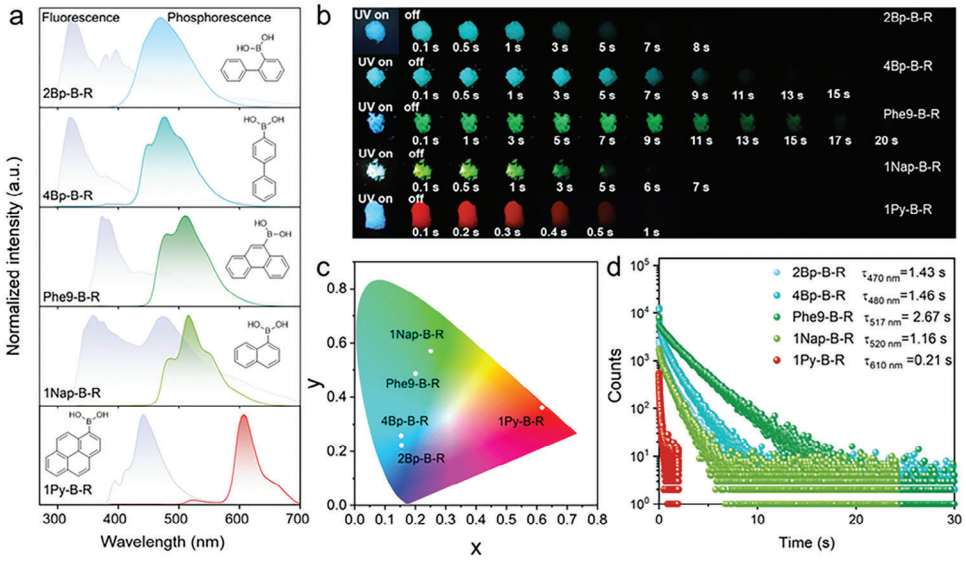

Figure 2. Photophysical properties of RTP cellulose. a) The steady-state photoluminescence and phosphorescence spectra of 2Bp-B-R ($\lambda_{ex} = 254$ nm), 4Bp-B-R ($\lambda_{ex} = 254$ nm), Phe9-B-R ($\lambda_{ex} = 310$ nm), 1Nap-B-R ($\lambda_{ex} = 310$ nm), and 1Py-B-R ($\lambda_{ex} = 365$ nm). b) Images of the long-lived RTP of arylboronic acids-RC. c) The CIE coordinate diagram and d) phosphorescence lifetimes of the arylboronic acids-RC.

excitation/time dependent color-variable afterglows, these RTP cellulose materials were employed in advanced technical applications for afterglow inks, anti-counterfeiting, information security and encryption, delay lighting, light panels of afterglow display. The work will shed new light on designing long-lived RTP materials with color-tunable afterglows. Moreover, the facile fabrication processes of the RTP cellulose were completed based in pure water, which is environmentally friendly and highly promising to be commercialized.

2. Results and Discussion

2.1. Construction of full-Color Tunable RTP Cellulose via Click Chemistry

As shown in Figure 1a, cellulose was reconstructed by directed redox strategy (Figure S1, Supporting Information), after which the RTP lifetime of cellulose is boosted from 78 to 799 ms (Figures S2 and S3, Supporting Information) due to the formation of more rigid microenvironment (Figure S4, Supporting Information). The Fourier transform infrared (FT-IR) and X-ray photoelectron spectroscopy (XPS) analyses illustrate the successful preparation of RC (Figure S5, Supporting Information). The 2,3-dialdehyde cellulose (DAC) is completely reduced by a non-measurable reaction with hydroxylamine and further supported by the disappear of the carbonyl peak in the FTIR. Therefore, the extra active primary hydroxyls in C2 and C3 positions are determined to be 11.07 mmol g^{-1} (Table S1, Supporting Information). A series of arylboronic acids can be facilely fixed to RC chains by facile B—O click reaction within 1 min in pure water, yielding color-tunable and long-lived cellulose, namely, 2Bp-B-R, 4Bp-B-R, Phe9-B-R, 1Nap-B-R, and 1Py-B-R, respectively (Figure 1a). The reaction yields were determined to be 45.3%, 32.43%, 45.4%, 42%, and 25% for 2Bp-B-R, 4Bp-B-R, Phe9-B-R, 1Nap-B-R, and 1Py-B-R, respectively (Figure S6, Supporting Information).

The photophysical properties of these five RTP cellulose were studied in detail (**Figure 2**). The steady-state photoluminescence and phosphorescence spectra of five RTP cellulose exhibit red-shifted emission with the expansion of π conjugation degrees from 2Bp-B-R/4Bp-B-R to Phe9-B-R/1Nap-B-R, then to 1Py-B-R (Figure 2a). Under UV irradiation, all the RTP cellulose emitted blue or cyan fluorescence; after ceasing the irradiation, full-color afterglows from blue to red even lasting for up to 20 s (Phe9-B-R) were observed, and the fluorescence and afterglow colors are consistent with the spectra (Figure 2b). The afterglow color variations were then recorded in Commission International de l'Eclairage (CIE) coordinate diagram, highly agreed well with the naked-eye observation (Figure 2c). Time-resolved emission decay curves indicate that the phosphorescence lifetime of Phe9-B-R is 2.67 s (Figure 2d), and the corresponding phosphorescence quantum yield is 9.37% (Figure S7, Supporting Information), superior to most of the reported natural or petroleum polymer based RTP materials (Figure S8 and Table S2, Supporting Information).[4,14,16,21] Other arylboronic acids-RC also show excellent performances, the lifetimes and the corresponding phosphorescence quantum yields of 2Bp-B-R, 4Bp-B-R, 1Nap-B-R, and 1Py-B-R are 1.43 s and 1.33%, 1.46 s and 3.01%, 1.16 s and 7.08%, 0.21 s and 0.84%, respectively (Figure 2d; Figures S9–S12, Supporting Information).

2.2. Full-Color Tunable Afterglows of RTP Cellulose

Intriguingly, further inspection of the RTP afterglow colors after switching off the different excitation sources pointed to the excitation-dependent characteristics (**Figures 3**a–d; Figure S13, Supporting Information). Taking 4Bp-B-R for example, after switching off 254 nm UV light, it displays sky-blue phosphorescence (Figure 3a). However, when the light switches to 310 or 365 nm, the afterglow colors transform from sky-blue to

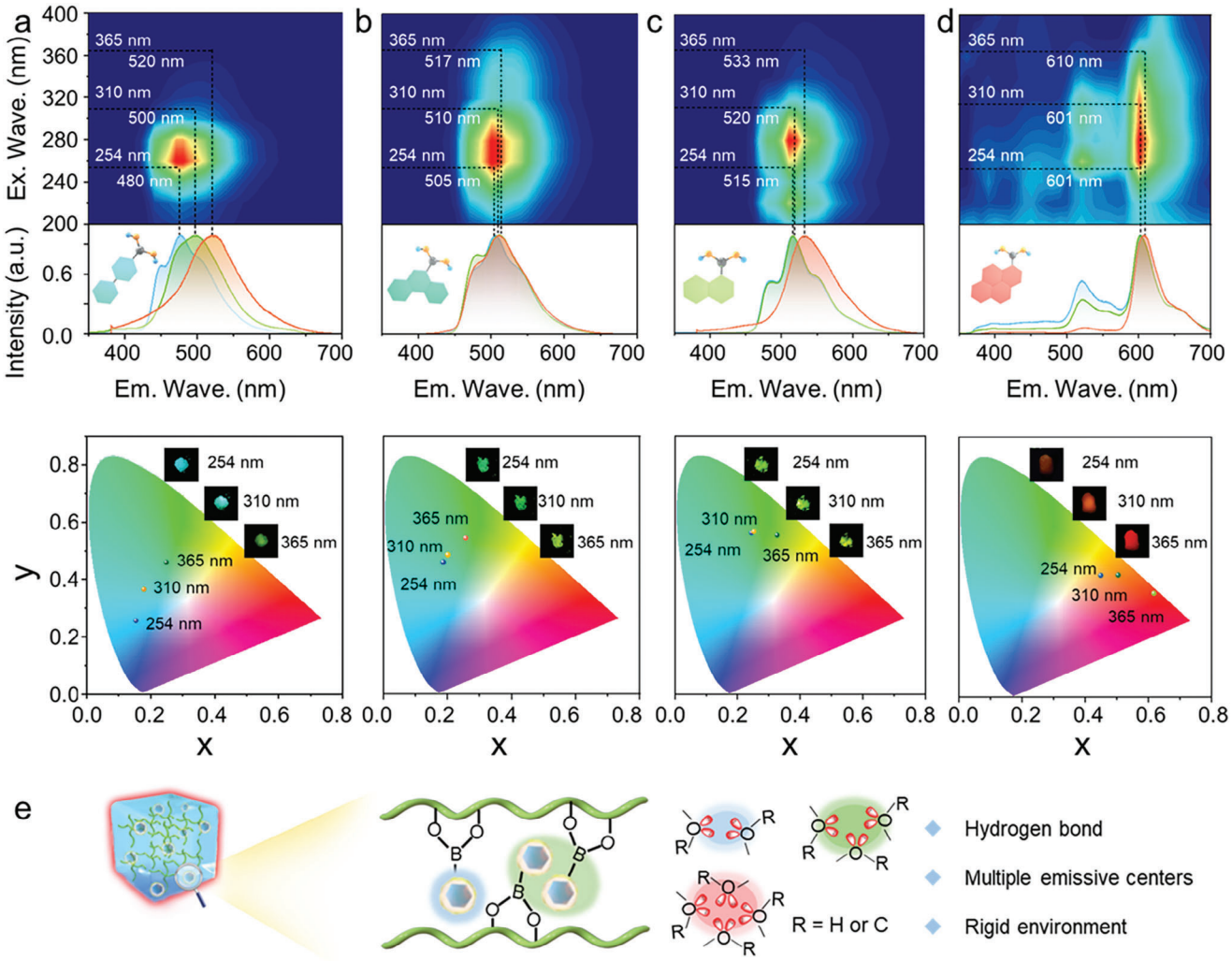

Figure 3. Excitation-dependent RTP of arylboronic acids-RC. Excitation-phosphorescence mapping, phosphorescence spectra, CIE coordinate diagrams of full-color tunable afterglows under different λ_{ex} for a) 4Bp-B-R, b) Phe9-B-R, c) 1Nap-B-R, and d) 1Py-B-R. Inset: Photographs of afterglows after removing the different excitation sources. e) Schematic illustration of multiple emissive species for the origination of full-color tunable afterglows in arylboronic acids-RC (Ex. Wave.: excitation wavelength, Em. Wave.: emission wavelength).

cyan and then to greenish–yellow (Figure S13, Supporting Information). Such variations can also be clearly recognized from the excitation-phosphorescence mapping and phosphorescence spectra (Figure 3a). In detail, when excited by 254, 310, and 365 nm UV lights, the phosphorescence emission maxima of 4Bp-B-R could be adjusted from 480 to 500 nm and then to 520 nm, respectively. Accordingly, the CIE coordinates vary from (0.15, 0.26) to (0.18, 0.37) and then to (0.24, 0.46), which agree well with the above observation (Figure 3a). The emission decay lifetimes of 4Bp-B-R monitored at 254 nm and 310 nm excitation were measured to be 1.46 and 1.2 s (Figure 2d; Figure S14, Supporting Information), respectively, indicating the existence of diverse emissive species with diverse lifetimes.

Apart from 4Bp-B-R, other arylboronic acids-RC samples also present the similar excitation-dependent afterglow RTP (Figures 3b–d; Figure S15, Supporting Information). Due to the structural similarity between 2Bp-B-R and 4Bp-B-R, their excitation-dependent afterglows are almost the same with moderate variance (Figure S15, Supporting Information). For Phe9-B-R, distinct deep-green, green, and lemon lime afterglows are observed after ceasing 254, 310, and 365 nm UV irradiation, respectively (Figure 3b; Figure S13, Supporting Information). For 1Nap-B-R, as the λ_{ex} increase, the phosphorescence emission maxima change from 515 to 533 nm, corresponding to greenish–yellow to yellow afterglow evolution (Figure 3c). As for 1Py-B-R, the phosphorescence emission contains mainly two regions of 500–550 and 600–620 nm, the peaks located at 520 nm are suppressed with increased λ_{ex}, then the peak at about 610 nm becomes prominent. The CIE coordinates of afterglow colors change from orange (0.45, 0.42) to orange–red (0.50, 0.43) and then to red (0.62, 0.36) (Figure 3d). The above results demonstrate the full-color tunable afterglows of arylboronic acids-RC, which should be ascribed to presence of multiple clusterizations of aromatic and nonaromatic moieties with π/n electrons in the RC matrix.[22] As shown in Figure 3e, the tangled cellulose chain may also behave as matrices to immobilize the emitting centers

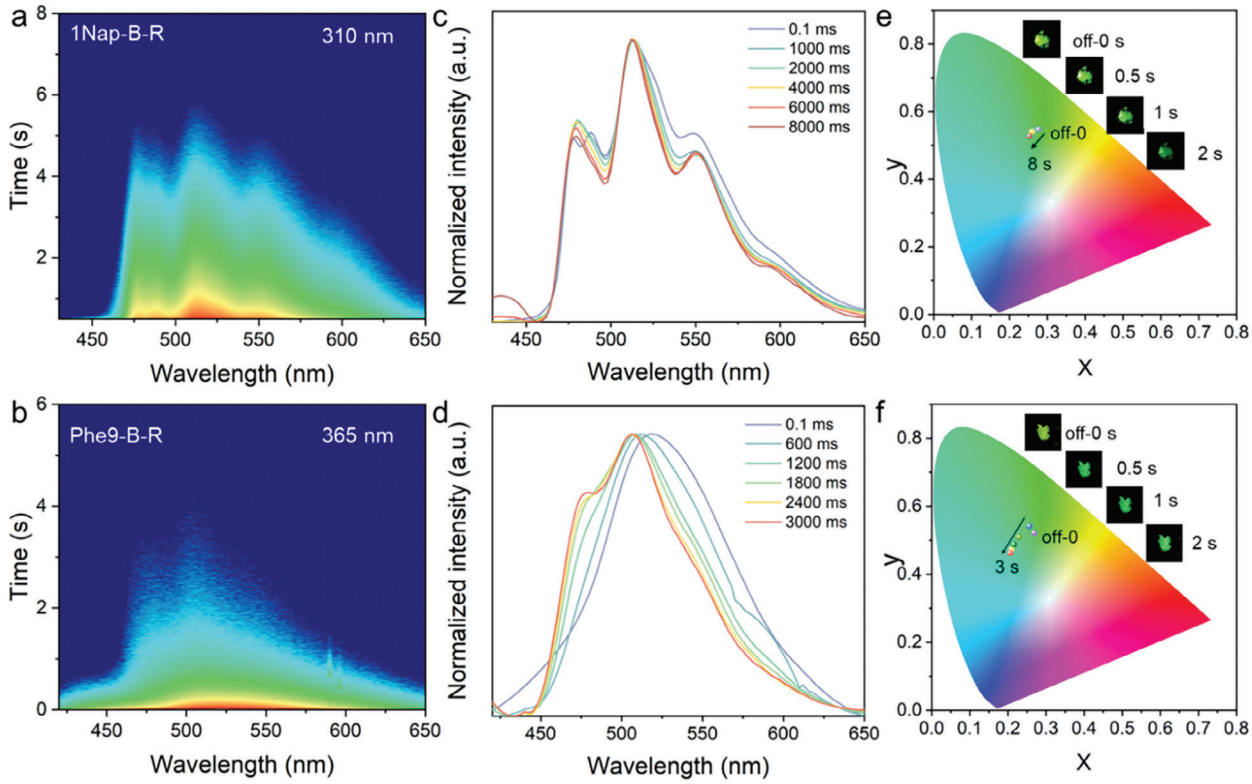

Figure 4. Time-dependent RTP of 1Nap-B-R and Phe9-B-R. Time-resolved afterglow mapping for a) 1Nap-B-R (λ_{ex} = 310 nm) and b) Phe9-B-R (λ_{ex} = 365 nm). Time-resolved emission spectra for c) 1Nap-B-R and d) Phe9-B-R. CIE coordinate diagrams of time-dependent afterglows for e) 1Nap-B-R and f) Phe9-B-R, respectively. Inset: digital pictures of the afterglow colors taken from off-0 to 2 s after removing the excitation source.

and thus to stabilize the excited triplet species by forming hydrogen bonds and B—O covalent bonds. The arylboronic acids-RC may form isolated monomer, dimer-like aggregate and clusters via through-space conjugations with the aid of cellulose chains and B—O covalent cross-linkage and hydrogen bonds, which have various energy levels and effective conjugation lengths. Thereby, some different clusters would dominate the RTP process and consequently afford color-variable afterglows with changing λ_{ex}.

It is remarkable that 1Nap-B-R and Phe9-B-R also display time-dependent color-variable afterglows after ceasing the 310 and 365 nm irradiation (t_{off}), and the afterglow color undergoes greenish–yellow (t_{off} = 0 s) to green (t_{off} = 2 s) variation for 1Nap-B-R and lemon lime (t_{off} = 0 s) to green (t_{off} = 2 s) variation for Phe9-B-R, respectively (**Figure 4**; Figure S13, Supporting Information). The unusual phenomenon encourages us to further map the transient photoluminescence decay images of 1Nap-B-R and Phe9-B-R (Figures 4a,b). As time evolves, the phosphorescence intensities for 1Nap-B-R and Phe9-B-R gradually decreases, and the relatively intensities show a hypochromatic shift trend in the emission profile (Figures 4c,d). The time-resolved emission spectra of 1Nap-B-R after ceasing 310 nm UV irradiation show a greenish afterglow with blue, green, and yellow phosphorescence bands with maxima at 480, 520, and 550 nm (t_{off} = 0.1 ms) (Figures 4c), respectively. With prolonged time, the relative intensity of yellow phosphorescence band (at 550 nm) gradually decreased, while the blue phosphorescence band (at 480 nm) gradually increased. The yellow emissive species with a lifetime of 0.44 s decay faster than the blue emissive species with a lifetime of 0.31 s (Figure S16, Supporting Information), resulting in a dynamic afterglow color evolution from greenish–yellow to green (Figure 4e). Similarly, the delayed emission of Phe9-B-R hypochromatic-shifts from 530, 517 to 480 nm with the time lapse (Figure 4d). Accordingly, the afterglow color of Phe9-B-R evolves from lemon lime to green after ceasing the UV irradiation. The CIE diagrams clearly confirm the afterglow color evolutions with delayed time, which are consistent with the naked eye observation and different emission decay lifetimes monitored at different wavelengths (Figure 4f; Figure S17, Supporting Information). Previously study demonstrated that time-dependent afterglows stemmed from the similar species with thermally active delayed fluorescence and phosphorescence emission.[23] The temperature-dependent delayed emission spectra of 1Nap-B-R display a gradual intensity increase as the temperature decreased from 298 to 77 K (Figure S18, Supporting Information), excluding the assignment of thermally active delayed fluorescence. So, time-dependent afterglows of 1Nap-B-R and Phe9-B-R should origin from distinct emissive species with diverse lifetimes (Figure 3e).

2.3. Mechanism for Long-Lived and Color-Tunable Afterglow

To validate the superiority and effectiveness of the proposed reconstruction and click chemistry strategy, a series of control

experiments were executed. First, the phosphorescence spectra of five arylboronic acids (2Bp-B, 4Bp-B, Phe9-B, 1Nap-B, and 1Py-B) were studied (Figure S19, Supporting Information), the five arylboronic acids didn't emit RTP themselves because the severe aggregation will quench the emission.[24] Once the arylboronic acids were anchored and dispersed in cellulose chains, the radiative transition channel will be activated. The delayed emission spectra of 2Bp-B, Phe9-B, 1Nap-B, and 1Py-B in tetrahydrofuran (THF) solution (10^{-5} M) at 77 K are consistence with arylboronic acids-RC at ambient environment, indicating that the arylboronic acid chromophores are the main emissive species in RTP cellulose (Figure S20, Supporting Information).

Then, the effect of the doping concentration and covalent anchoring on RTP was investigated. Taking Phe9-B-R with different doping concentrations (i.e., 0.5, 1, 5, 10, 20, 40, 100 wt.%, mass ratios of Phe9-B and RC) as an example, upon increasing the doping content, the phosphorescence intensities of Phe9-B-R increase to a maximum and then decrease (Figure S21, Supporting Information). It can be concluded that the excess Phe9-B will lead to energy dissipation and aggregation-caused quenching,[25] and the optimized concentration is determined to be 1 wt.%. FT-IR spectra were used to verify the presence of B—O covalent bonds in arylboronic acids-RC (Figures S22 and S23, Supporting Information). The doping concentration is kept at a high level (i.e., 40 wt.%) to make the peaks prominent, Phe9-B-R shows the characteristic covalent B—C and B—O—C peaks at 952 and 1046 cm^{-1}. The peaks located at 1105 and 1490 cm^{-1} are considered as the deformation vibrations of the plane B—OH and the stretching vibrations of B—O (Figure S23, Supporting Information).[26] The results are also in accordance with that of XPS spectra, in which C 1s and B 1s curves display covalent C—O—B at 288.61 eV and B—O at 192.1 eV (Figure S24, Supporting Information).[27] Moreover, boron, oxygen, and carbon elements are homogeneously distributed throughout Phe9-B-R in energy-dispersive X-ray spectroscopy images (Figure S25, Supporting Information). All the evidences point to the successfully formation of the B—O covalent bond between arylboronic acids and RC after the B—O click reaction.

Furthermore, control samples prepared with pristine microcrystalline cellulose and arylboronic acids (denoted as arylboronic acids-M), samples prepared with RC and aromatic chromophores without boronic acid groups (denoted as Bp-R, Phe-R, Nap-R, Py-R), and sample prepared with RC and aromatic chromophores with two boronic acid groups (here 4,4-biphenyldiboronic acid was adopted, the sample was denoted as 4,4-Bp-B-R) were obtained in sequence to further state the important role of B—O covalent interactions. The lifetimes of 2Bp-B-M, 4Bp-B-M, Phe9-B-M, 1Nap-B-M, and 1Py-B-M are 0.88, 1.34, 1.42, 0,81, and 0.19 s, respectively. The phosphorescence intensities, afterglow duration and phosphorescence lifetimes of arylboronic acids-M samples are obviously inferior to arylboronic acids-RC samples (Figures S26–S30, Supporting Information). The sharp contrasts state that due to the lack of water-solubility and active extracyclic primary hydroxyl groups, the formation of B—O bonds between arylboronic acids and microcrystalline cellulose is inadequate, the molecular motion dissipations cannot be effectively suppressed. On the other hand, bare aromatic chromophores lacking boronic acid groups could only be mixed into RC by physical interactions, causing the faint phosphorescence intensity and short lifetime of the samples (Figures S31–S34, Supporting Information). As such, the phosphorescence lifetimes are only 682, 633, 534, and 26 ms for Bp-R, Phe-R, Nap-R, and Py-R, respectively. The situation is completely different in 4,4-Bp-B-R, the afterglow duration, phosphorescence intensity, and phosphorescence lifetime (from 1.46 to 1.53 s) of which are simultaneously improved compared with 4Bp-B-R (Figures S35–S37, Supporting Information).

Last, to deeply explore the enhancement effect on RTP provided by covalent interactions, other five samples were prepared (denoted as 2Bp-B-R-C, 4Bp-B-R-C, Phe9-B-R-C, 1Nap-B-R-C, and 1Py-B-R-C). The only distinction in the preparation process is that alkali is not added to catalyze the reaction between arylboronic acids and RC. The control samples exhibit similar excitation-dependent RTP, but the phosphorescence lifetimes of 2Bp-B-R-C/4Bp-B-R-C/Phe9-B-R-C/1Nap-B-R-C/1Py-B-R-C are shortened from 1.43, 1.46, 2.67, 1.16, and 0.21 s to 0.32, 1.3, 0.91, 1.05 and 0.1 s (Figures S38–S42, Supporting Information). It should be noted that the UV–vis absorbance spectra of the arylboronic acids-RC samples with alkali catalysis show redshift absorbance compared with the control samples (**Figure 5**a), which could be ascribed to the formation of more B—O covalent bonds in alkali environments. The formation of the B—O covalent bond conducive to π–π stacking, leading to increasing the degree of intermolecular conjugation. The π–π* transitions require a lower energy and longer wavelength of excitation light. Therefore, the phosphorescence intensities and lifetimes of arylboronic acids-RC are superior to the control samples. To sum up, active hydroxyl groups of RC can end-cap arylboronic acids via B—O covalent bonds, resulting in the restriction of the thermal motions and rotations of the phenyl rings and boosted RTP performances (Figure 1a).[28]

Density functional theory (DFT) calculations were carried out to figure out the internal mechanism of remarkable RTP properties of arylboronic acids-RC. As discussed above, the arylboronic acid chromophores are the main emissive species in arylboronic acids-RC, thus the energy levels of the first singlet excited state (S_1) and the first triplet excited state (T_1) for five arylboronic acids were calculated as theoretical models (Figure S43, Supporting Information). As shown in Figure 5b, the RTP transition energy gaps (T_1–S_0) show a gradually decreasing trend with the extended π conjugation degree, which is the reason why arylboronic acids-RC show redshifted and full-color tunable RTP emission. Additionally, taking S_1 state of Phe9-B for example, we calculated the rate constant of Phe9-B-R to understand the detailed ISC processes. The ISC constant (k_{isc}) is as large as 4.4×10^7 s^{-1}, which is almost two times higher than the radiative rate constant of fluorescence ($k_{f,r}$) and is conducive to boost singlet–triplet intersystem crossing and phosphorescent quantum yield of Phe9-B-R based on the equation of $\Phi_p = k_{isc} \times \tau_f \times k_{p,r} \times \tau_p$ (Table S3, Supporting Information). Meanwhile, the complete overlap of the hole and the particle of the T_1 points to a typical locally excited (LE) transition, which makes the phosphorescence transition (T_1–S_0) difficult and results in a small spin-orbit coupling value and phosphorescent radiative transition constant ($k_{p,r}$) (Figure 5c). Consequently, the RTP lifetime (τ_p) of Phe9-B-R could be prolonged according to the equation of $\tau_p = 1/(k_{p,r} + k_{p,nr})$. Indeed, the $k_{p,r}$ and $k_{p,nr}$ of Phe9-B-R are determined to be just 0.056 and 0.318 s^{-1} (Table S3, Supporting

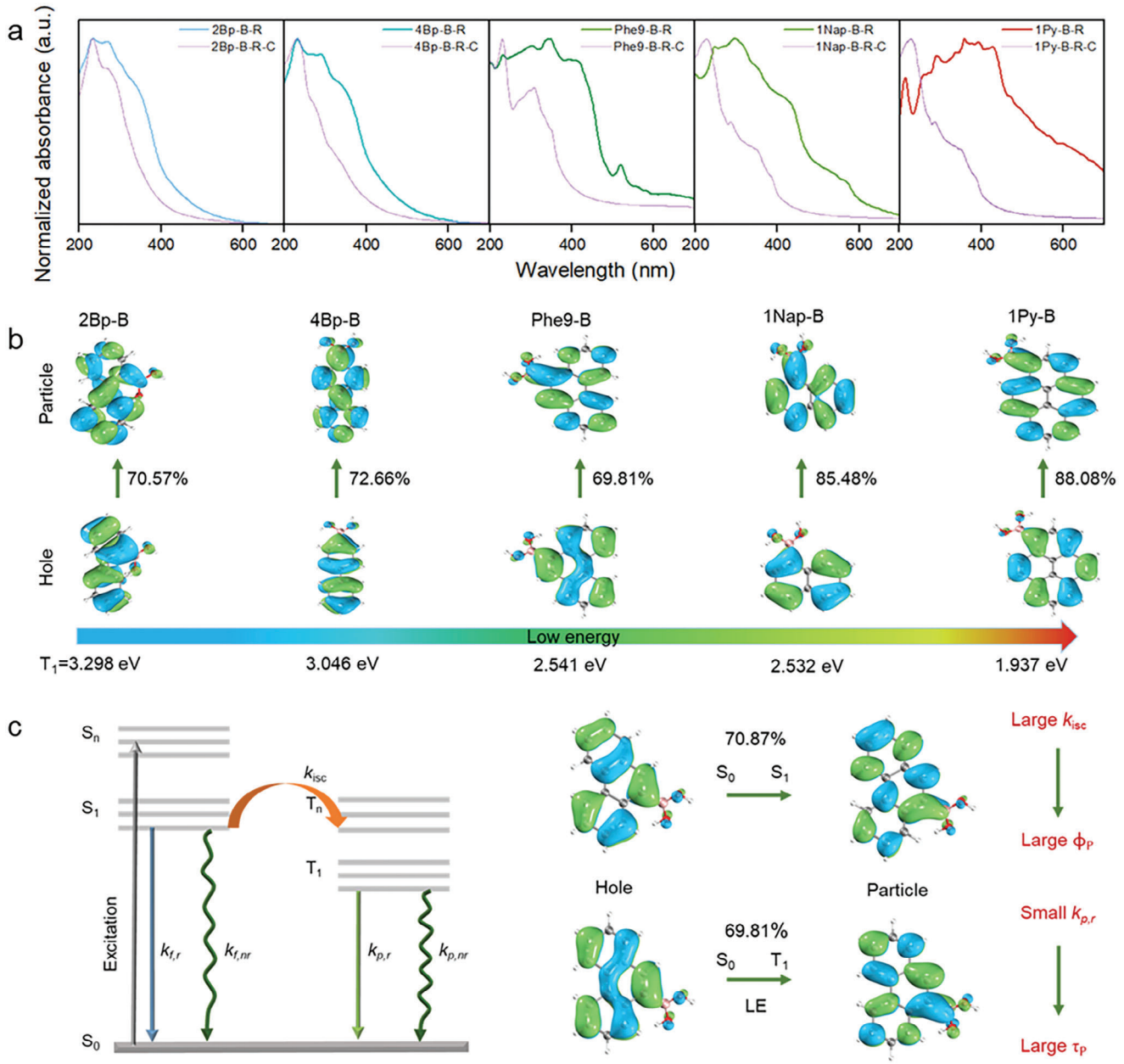

Figure 5. The mechanism for long-lived and color-tunable RTP cellulose. a) The UV–vis absorbance spectra of 2Bp-B-R, 4Bp-B-R, Phe9-B-R, 1Nap-B-R, 1Py-B-R, and the corresponding control samples. b) The theoretical calculations about natural transition orbitals (NTOs) of 2Bp-B, 4Bp-B, Phe9-B, 1Nap-B, and 1Py-B. c) The Jablonski diagram and the NTOs of Phe9-B.

Information), which are well consistent with the theoretical results and demonstrated the feasibility of the above mechanisms.[17b,29]

2.4. Applications of Full-Color Tunable RTP Cellulose

Taking advantage of the distinguishable long-lived full-color tunable afterglows and excellent water solubility (Figure S44, Supporting Information), these environmentally friendly RTP cellulose can be used for nontoxic afterglow inks, delay lighting, and afterglow display. First, a part of the petals of a paper flower was soaked in 2Bp-B-R aqueous solution, and then a beautiful deep blue fluorescence decorative flower was emerged upon UV illumination (**Figure 6**a). The paper flower turned as a sky-blue car logo when the UV lamp was turned off. Different patterns such as green afterglow flower and multicolor afterglow snail can be drawn using RTP cellulose inks (Figure 6a). These phosphorescence inks that are not able to be photocopied, but are readable only under special conditions. Regarding the excitation-dependent afterglow characteristic of Phe9-B-R and 1Py-B-R, a high-level information encryption is presented. The aqueous

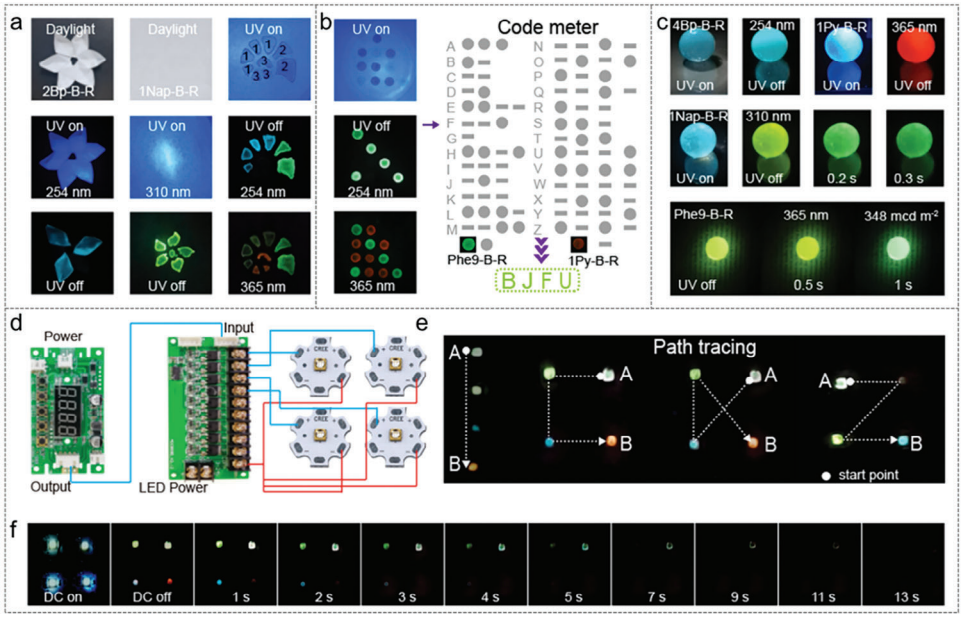

Figure 6. Applications of full-color tunable RTP cellulose. a) Left: flower petals painted by 2Bp-B-R, middle: flower painted by 1Nap-B-R ink in A4 paper, right: multicolor snail painted by RTP cellulose inks (1: 4Bp-B-R, 2: Phe9-B-R, 3: 1Py-B-R). b) Information encryption with Morse code using different RTP cellulose inks. c) Various colors of delay lighting luminous pearls made by different RTP cellulose. d) Circuit diagram of afterglow display device. e) Path tracing from A to B with multicolor afterglows by controlling direct current (DC) on and off. f) Demonstration of afterglow display made of full-color RTP cellulose (2Bp-B-R, 1Nap-B-R, Phe9-B-R, and 1Py-B-R).

solutions of Phe9-B-R and 1Py-B-R were used as inks to denote as "•" and "▬" on A4 paper. When irradiated with 254 or 365 nm UV lights, no information could be seen on the paper and the information is encrypted. The information "•" emerged until removing the 254 nm excitation source, but the information is still encrypted since the RTP emission of 1Py-B-R was inactive. Only after switching off the 365 nm UV, the lemon lime and red afterglows of Phe9-B-R and 1Py-B-R could be identified, acquiring information "•" and "▬" simultaneously (Figure 6b). The integrated Morse code could be obtained by following the complete afterglow information on the paper. Then, the hidden information "BJFU" could be read according to the Morse code meter (Figure 6b). The excitation-dependent color-variable afterglow of RTP cellulose offers additional protection for multi-mode anti-counterfeiting application and multi-coding procedures for high-level information encryption.

Furthermore, RTP cellulose could be encapsulated in transparent substrate (here polydimethylsiloxane (PDMS) was used as a demo) to fabricate luminous pearls for delay lighting. Homogeneous and colorful delay lighting luminous pearls glow brightly in the dark (Figure 6c; Movie S1, Supporting Information). The dynamically color-variable luminous pearls made of 1Nap-B-R or Phe9-B-R show the first channel greenish–yellow and lemon lime afterglows at 0.2 and 0.5 s, which evolve to the second channel green afterglows at 0.3 and 1 s, respectively (Figure 6c; Movies S1 and S2, Supporting Information). Remarkably, the afterglow absolute luminance of Phe9-B-R luminous pearl is 348 mcd m^{-2}, capable of illuminating the information in the dark, and the afterglow sustains for > 10 s, highly promising for delay lighting.

Finally, RTP cellulose could also be used as electroluminescent panels for afterglow displays (Figure 6d). The RTP cellulose can be used in conjunction with electrical stimulation for afterglow displays, which can be manufactured by integrating the multicolor phosphorescence cellulose material on a circuit diagram-controlled photoelectric device. Using manipulating the direct current, different paths displaying colorful afterglows from blue to red could be clearly traced by the naked eye after turning off the power source (Figure 6e; Movie S3, Supporting Information). The integrated electroluminescent device also exhibits colorful afterglows with time (Figure 6f; Movie S4, Supporting Information). The photoelectric devices decorated by RTP cellulose demonstrate potential applications for afterglow display and path tracking.

3. Conclusion

In summary, we developed an ingenious design strategy to facilely prepare RTP cellulose with long-lived and full-color tunable afterglows. Cellulose was reconstructed by directed redox to afford ample active hydroxyl groups in molecular skeleton and to anchor chromophores with various π conjugations via click chemistry within 1 min in pure water. The highly rigid microenvironment provided by B—O covalent bonds and hydrogen bonds can restrict the thermal motions to stabilize the triplet excitons, thus the target RTP cellulose displays a ultralong phosphorescence lifetime of 2.67 s, a high phosphorescence quantum yield of 9.37%, and a striking absolute afterglow luminance of 348 mcd m^{-2} simultaneously. Due to the formation of various emissive species, the smart RTP cellulose also affords excitation- and time-dependent afterglows. The environmentally friendly RTP cellulose show promising applications in nontoxic afterglow inks, delay lighting, and afterglow display. The development of

the RTP cellulose will broaden multifunctional afterglow materials and expand applications of cellulose in much more fields.

4. Experimental Section

Materials: Unless other noted, all reagents were purchased from commercial sources without further purification. 2-Biphenylboronic acid (purity: 97%), 4-biphenylboronic acid (purity: 98%), 1-naphthylbornic acid (purity: 97%), 1-pyrenylboronic acid (purity: 95%), 9-phenanthracenylboronic acid (purity: 97%), MCC (microcrystalline cellulose, 50 μm), sodium periodate, and ethylene glycol were obtained from Macklin (Shanghai) without further purification. Sodium borohydride ($NaBH_4$) was purchased from Guangdong Guanghua Chemical Factory Co., ltd.

Synthesis of Reconstructed Cellulose (RC): Cellulose (31.68 g) and $NaIO_4$ (75.29 g) (molar ratio of 1:2) were added to deionized water (800 mL) and stirred under the dark environment for 12 h at 60 °C. The reaction was stopped by a certain amount of ethylene glycol (80 mL) and the oxidized cellulose was dialyzed to remove impurities. Then, $NaBH_4$ (1.2 g) was added to the oxidized cellulose solution (3 g, 100 mL) and stirred for 4 h at ambient temperature. The RC solid was obtained by dialysis and freeze drying.

Synthesis of Arylboronic Acids-RC: RC (100 mg) was dissolved in 0.6 mL deionized water in a glass bottle, 2-biphenylboronic acid/4-biphenylboronic acid/1-naphthylbornic acid/9-phenanthracenylboronic acid/1-pyrenylboronic acid (1 mg in 0.8 mL water) and ammonium hydroxide (0.2 mL) were subsequently added. Then, the mixture solutions were stirred at 80°C for 1 min and the products were obtained by freeze drying.

Preparation of RTP Cellulose Inks: 2Bp-B-R, 4Bp-B-R, 1Nap-B-R, Phe9-B-R, and 1Py-B-R were dissolved in deionized water to form a uniform solution (50 mg mL^{-1}). The as prepared inks were directly used for pattern painting.

Preparation of Afterglow Displays: 2Bp-B-R, 4Bp-B-R, 1Nap-B-R, Phe9-B-R, and 1Py-B-R were grinded into uniform powder and mixed with PDMS matrix at a mass ratio of 1:10, respectively. The mixture was coated on the LED surface. The device was finally molded at 80 °C for 4 h to obtain the afterglow displays.

Measurements: UV–vis absorbance spectra were collected using a Shimadzu UV-3600. Fourier transform infrared (FT-IR) spectra were recorded by Bruker OPTIK GmbH Tensor II equipment (Bruker, Germany) from 500 to 4000 cm^{-1}. X-ray photoelectron spectroscopy (XPS) spectra were measured using a Thermo Scientific K-Alpha spectrometer with a 200 W monochromatic Al Kα radiation. Steady-state photoluminescence spectra and phosphorescence spectra were obtained using a Hitachi F-7100 fluorescence spectrophotometer. The delayed emission spectra at 77 K were measured on an Edinburgh FLS 1000 instrument. The phosphorescence lifetimes, photoluminescence quantum yields and time-resolved emission spectra were measured using an Edinburgh FLS 980 instrument with a microsecond flash-lamp (uF2) and an integrating sphere (150 mm in diameter), respectively. The absolute afterglow luminance was measured by a PR-305 detector (excitation time: 10 s; steady state interval: 1 s; scan time: 2 min). The afterglow photos and videos were taken using a HUAWEI P40 pro mobile phone under ambient conditions. Samples in the form of powder was used to measure the photophysical properties.

Theoretical Calculation: All the theoretical calculations were performed using the Gaussian 16 program. The NTOs of S_1 and T_1 state for 2Bp-B, 4Bp-B, Phe9-B, 1Nap-B, and 1Py-B were obtained by electron excitation analysis from the transition density matrix of time-dependent density functional theory (TD-DFT) calculation using Multiwfn program.

Supporting Information

Supporting Information is available from the Wiley Online Library or from the author.

Acknowledgements

This work was supported by the National Science Fund for Distinguished Young Scholars of China (32225034), National Natural Science Foundation of China (22308028), State Key Laboratory of Pulp and Paper Engineering (202308), and Fundamental Research Funds for the Central Universities (QNTD202302, BLX202131).

Conflict of Interest

The authors declare no conflict of interest.

Data Availability Statement

The data that support the findings of this study are available from the corresponding author upon reasonable request.

Keywords

cellulose, click chemistry, directed redox, full-color tunable afterglow, room temperature phosphorescence

Received: October 10, 2023
Revised: October 30, 2023
Published online:

[1] a) X. Yao, H. Ma, X. Wang, H. Wang, Q. Wang, X. Zou, Z. Song, W. Jia, Y. Li, Y. Mao, M. Singh, W. Ye, J. Liang, Y. Zhang, Z. Liu, Y. He, J. Li, Z. Zhou, Z. Zhao, Y. Zhang, G. Niu, C. Yin, S. Zhang, H. Shi, W. Huang, Z. An, *Nat. Commun.* **2022**, *13*, 4890; b) J. Wei, B. Liang, R. Duan, Z. Cheng, C. Li, T. Zhou, Y. Yi, Y. Wang, *Angew. Chem., Int. Ed.* **2016**, *55*, 15589; c) G. Xie, J. Wang, X. Xue, H. Li, N. Guo, H. Li, D. Wang, M. Li, W. Huang, R. Chen, Y. Tao, *Appl. Phys. Rev.* **2022**, *9*, 031410.

[2] a) W. Ye, H. Ma, H. Shi, H. Wang, A. Lv, L. Bian, M. Zhang, C. Ma, K. Ling, M. Gu, Y. Mao, X. Yao, C. Gao, K. Shen, W. Jia, J. Zhi, S. Cai, Z. Song, J. Li, Y. Zhang, S. Lu, K. Liu, C. Dong, Q. Wang, Y. Zhou, W. Yao, Y. Zhang, H. Zhang, Z. Zhang, X. Hang, et al., *Nat. Mater.* **2021**, *20*, 1539; b) Q.-C. Zhang, H. Xiao, X. Zhang, L.-J. Xu, Z.-N. Chen, *Coord. Chem. Rev.* **2019**, *378*, 121.

[3] a) B. Lü, Q. Gao, P. Li, J. Rao, Z. Lv, M. Shi, Y. Hu, X. Hao, G. Chen, M. Yin, F. Peng, *Cell. Rep. Phys. Sci.* **2022**, *3*, 101015; b) D. Jiang, C. Du, Z. Yan, S. Ge, Z. Feng, L. Wan, P. Lu, *J. Mater. Chem. C* **2023**, *11*, 4203; c) D. Wang, J. Gong, Y. Xiong, H. Wu, Z. Zhao, D. Wang, B. Z. Tang, *Adv. Funct. Mater.* **2023**, *33*, 2208895.

[4] a) Y. Zhou, W. Qin, C. Du, H. Gao, F. Zhu, G. Liang, *Angew. Chem., Int. Ed.* **2019**, *58*, 12102; b) Y. Zhang, X. Chen, J. Xu, Q. Zhang, L. Gao, Z. Wang, L. Qu, K. Wang, Y. Li, Z. Cai, Y. Zhao, C. Yang, *J. Am. Chem. Soc.* **2022**, *144*, 6107.

[5] M. Cui, P. Dai, J. Ding, M. Li, R. Sun, X. Jiang, M. Wu, X. Pang, M. Liu, Q. Zhao, B. Song, Y. He, *Angew. Chem., Int. Ed.* **2022**, *61*, e202200172.

[6] a) X. Ma, C. Xu, J. Wang, H. Tian, *Angew. Chem., Int. Ed.* **2018**, *57*, 10854; b) M. Baroncini, G. Bergamini, P. Ceroni, *Chem. Commun.* **2017**, *53*, 2081.

[7] a) L. Gu, H. Shi, L. Bian, M. Gu, K. Ling, X. Wang, H. Ma, S. Cai, W. Ning, L. Fu, H. Wang, S. Wang, Y. Gao, W. Yao, F. Huo, Y. Tao, Z. An, X. Liu, W. Huang, *Nat. Photon.* **2019**, *13*, 406; b) J. Yang, Y. Zhang, X. Wu, W. Dai, D. Chen, J. Shi, B. Tong, Q. Peng, H. Xie, Z. Cai, Y. Dong, X. Zhang, *Nat. Commun.* **2021**, *12*, 4883.

[8] a) W.-W. Xu, Y. Chen, Y.-L. Lu, Y.-X. Qin, H. Zhang, X. Xu, Y. Liu, *Angew. Chem., Int. Ed.* **2022**, *61*, e202115265; b) L. Bian, H. Shi, X. Wang, K. Ling, H. Ma, M. Li, Z. Cheng, C. Ma, S. Cai, Q. Wu, N. Gan, X. Xu, Z. An, W. Huang, *J. Am. Chem. Soc.* **2018**, *140*, 10734.

[9] a) Z. Wang, Y. Zhang, C. Wang, X. Zheng, Y. Zheng, L. Gao, C. Yang, Y. Li, L. Qu, Y. Zhao, *Adv. Mater.* **2020**, *32*, 1907355; b) X. Meng, Q. Hu, X. Wang, T. Ma, W. Liu, X. Zhu, C. Ye, *J. Mater. Chem. C* **2022**, *10*, 17620.

[10] a) S. Tang, Z. Zhao, J. Chen, T. Yang, Y. Wang, X. Chen, M. Lv, W. Z. Yuan, *Angew. Chem., Int. Ed.* **2022**, *61*, e202117368; b) Z. An, C. Zheng, Y. Tao, R. Chen, H. Shi, T. Chen, Z. Wang, H. Li, R. Deng, X. Liu, W. Huang, *Nat. Mater.* **2015**, *14*, 685.

[11] a) P. Data, M. Okazaki, S. Minakata, Y. Takeda, *J. Mater. Chem. C* **2019**, *7*, 6616; b) Z.-A. Yan, X. Lin, S. Sun, X. Ma, H. Tian, *Angew. Chem., Int. Ed.* **2021**, *60*, 19735.

[12] a) W. Shao, J. Kim, *Acc. Chem. Res.* **2022**, *55*, 1573; b) Z. Wu, J. Nitsch, T. B. Marder, *Adv. Opt. Mater.* **2021**, *9*, 2100411.

[13] a) L.-L. Du, B.-L. Jiang, X.-H. Chen, Y.-Z. Wang, L.-M. Zou, Y.-L. Liu, Y.-Y. Gong, C. Wei, W.-Z. Yuan, *Chin. J. Polym. Sci.* **2019**, *37*, 409; b) Z. Zhu, L. Zeng, W. Li, D. Tian, W. Xu, *ACS Sustainable Chem. Eng.* **2021**, *9*, 17420.

[14] a) X. Zhang, Y. Cheng, J. You, J. Zhang, C. Yin, J. Zhang, *Nat. Commun.* **2022**, *13*, 1117; b) X. Zhang, C. Yin, J. You, R. Li, J. Zhang, Y. Cheng, Y. Wang, J. Zhang, *Research* **2023**, *6*, 0029; c) X. Zhang, Y. Cheng, J. You, J. Zhang, Y. Wang, J. Zhang, *ACS Appl. Mater. Interfaces* **2022**, *14*, 16582; d) X. Zhang, J. You, J. Zhang, C. Yin, Y. Wang, R. Li, J. Zhang, *CCS Chem.* **2022**, 2140.

[15] D. Li, J. Yang, M. Fang, B. Z. Tang, Z. Li, *Sci. Adv.* **2022**, *8*, eabl8392.

[16] Q. Gao, J. Rao, Z. Lv, M. Shi, M. Chen, G. Chen, X. Hao, B. Lü, F. Peng, *Chem. Eng. J.* **2023**, *451*, 138923.

[17] a) R. Tian, S. Gao, K. Li, C. Lu, *Nat. Commun.* **2023**, *14*, 4720; b) R. Tian, S.-M. Xu, Q. Xu, C. Lu, *Sci. Adv.* **2020**, *6*, eaaz6107.

[18] D. Li, Y. Yang, J. Yang, M. Fang, B. Z. Tang, Z. Li, *Nat. Commun.* **2022**, *13*, 347.

[19] C. Ren, Z. Wang, H. Ou, T. Wang, Z. Zhao, Y. Wei, H. Yuan, Y. Tan, W. Z. Yuan, *Small Methods* **2023**, 2300243.

[20] a) Y. Gao, Q. Zhang, F. Wang, P. Sun, *Chem. Eng. J.* **2023**, *471*, 144665; b) M. Zeng, T. Li, Y. Liu, X. Lin, X. Zu, Y. Mu, L. Chen, Y. Huo, Y. Qin, *Chem. Eng. J.* **2022**, *446*, 136935.

[21] a) Y. Zhang, Y. Su, H. Wu, Z. Wang, C. Wang, Y. Zheng, X. Zheng, L. Gao, Q. Zhou, Y. Yang, X. Chen, C. Yang, Y. Zhao, *J. Am. Chem. Soc.* **2021**, *143*, 13675; b) Y. Zhang, L. Gao, X. Zheng, Z. Wang, C. Yang, H. Tang, L. Qu, Y. Li, Y. Zhao, *Nat. Commun.* **2021**, *12*, 2297.

[22] X. Dou, T. Zhu, Z. Wang, W. Sun, Y. Lai, K. Sui, Y. Tan, Y. Zhang, W. Z. Yuan, *Adv. Mater.* **2020**, *32*, 2004768.

[23] a) J. Chen, T. Yu, E. Ubba, Z. Xie, Z. Yang, Y. Zhang, S. Liu, J. Xu, M. P. Aldred, Z. Chi, *Adv. Opt. Mater.* **2019**, *7*, 1801593; b) J.-X. Wang, Y.-G. Fang, C.-X. Li, L.-Y. Niu, W.-H. Fang, G. Cui, Q.-Z. Yang, *Angew. Chem., Int. Ed.* **2020**, *59*, 10032; c) Z. Wang, A. Li, Z. Zhao, T. Zhu, Q. Zhang, Y. Zhang, Y. Tan, W. Z. Yuan, *Adv. Mater.* **2022**, *34*, 2202182.

[24] J. Mei, N. L. C. Leung, R. T. K. Kwok, J. W. Y. Lam, B. Z. Tang, *Chem. Rev.* **2015**, *115*, 11718.

[25] N. Gan, H. Shi, Z. An, W. Huang, *Adv. Funct. Mater.* **2018**, *28*, 1802657.

[26] a) D. Wang, Z. Lu, X. Qin, Z. Zhang, Y.-E. Shi, J. W. Y. Lam, Z. Wang, B. Z. Tang, *Adv. Opt. Mater.* **2022**, *10*, 2200629; b) Q. Feng, Z. Xie, M. Zheng, *Chem. Eng. J.* **2021**, *420*, 127647; c) Y.-C. Liang, Q. Cao, K.-K. Liu, X.-Y. Peng, L.-Z. Sui, S.-P. Wang, S.-Y. Song, X.-Y. Wu, W.-B. Zhao, Y. Deng, Q. Lou, L. Dong, C.-X. Shan, *ACS Nano* **2021**, *15*, 16242.

[27] a) E. A. Il'inchik, V. V. Volkov, L. N. Mazalov, *J. Struct. Chem.* **2005**, *46*, 523; b) X. Zheng, Y. Huang, W. Lv, J. Fan, Q. Ling, Z. Lin, *Angew. Chem., Int. Ed.* **2022**, *61*, e202207104.

[28] Y. Liu, C. Deng, L. Tang, A. Qin, R. Hu, J. Z. Sun, B. Z. Tang, *J. Am. Chem. Soc.* **2011**, *133*, 660.

[29] a) W. Z. Yuan, X. Y. Shen, H. Zhao, J. W. Y. Lam, L. Tang, P. Lu, C. Wang, Y. Liu, Z. Wang, Q. Zheng, J. Z. Sun, Y. Ma, B. Z. Tang, *J Phys Chem* **2010**, *114*, 6090; b) W. Zhao, T. S. Cheung, N. Jiang, W. Huang, J. W. Y. Lam, X. Zhang, Z. He, B. Z. Tang, *Nat Commun.* **2019**, *10*, 1595.